

As part of the development approach of new research systems in oceanography, the research team of Oceanography and Coastal Processes of the IAMC-CNR – Oristano presents a report on the first application of the ocean model Fluidity-ICOM.

A modelling study of the barotropic tidal dynamics in the Strait of Messina.

Quattrocchi G.[1], Gorman G. [2], Piggott M. D. [2], Cucco A.[1]

[1] Istituto per l'Ambiente Marino Costiero, Consiglio Nazionale delle Ricerche, Oristano, Italy.
[2]Applied Modelling and Computation Group, Imperial College London, London, UK.
corresponding author: giovanni.quattrocchi@iamc.cnr.it

Abstract

This paper is devoted to a model case study of the barotropic tidal dynamics. A non-hydrostatic (i.e. fully three dimensional) ocean model, based on the finite-element method was applied in the Strait of Messina (Italy), where intense tidal flows interact with complex geometries of coasts and bathymetry. A simplified model configuration including only the tidal signal at the open boundaries was able to provide evidences that the barotropic tides, interacting with coastlines and bottom topography in such narrow sea strait, generate high amplitude overtones of the main tidal constituents as well as relatively intense tide-induced residual circulations. The spatial and temporal distribution of tidal flows was analysed with a numerical simulation of a whole synodic month. The vertical component of tidal flows, explicitly computed, was shown in cross-sections in order to emphasized the direct effect of boundaries constraints on the vertical acceleration. The presented model results endorse previous model approaches and observations and they remind the significance of the barotropic tidal dynamics in this domain of investigation.

Keywords

Non-hydrostatic; finite-element model; coastal sea; sea straits; barotropic tidal dynamics; tide induced residual circulation.

1. Introduction

The aim of this paper is to investigate the main features of the barotropic tidal dynamics in the Strait of Messina (Italy), where intense tidal flows interact with convolute boundary geometries. With this intent a model case study was carried out by using the Imperial College Ocean Model, named Fluidity-ICOM (Ford et al. 2004a, 2004b). It is a non-hydrostatic ocean model, based on the finite-element method that uses unstructured mesh to discretize the three-dimensional model domain.

Beyond the importance of measure and predict time, height and extent of water rises and falls of tides, for people or ships safety, constructions and emergency preparedness, the interaction between tides, geomorphologic constraints and averaged three-dimensional sea circulation is of primary interest for research. Shallow waters, sea straits or channels that are adjacent to wide basins are sensitive areas where co-oscillations, promoted by nonlinear distortion of the major tidal constituents (Le Provost et al., 1981), and tide-induced residual circulation profoundly affect the oceanographic state at different phenomenological scales. At straits and shallows advective processes dominate the dynamics (Cucco et al. 2016). The interaction between advection and physical constraints is able to generate vortices, formed gyres and residual circulation, whose features can be investigated by mean of a conceptual barotropic ocean model.

The singularity of the physical processes occurring in the Strait of Messina (hereafter SoM) is certainly known before its citation in Homer's epic and the modern science has already shown the scientific relevance of this area for oceanographic and ecological studies (Battaglia et al. 1995). The SoM is located in the Mediterranean Sea, between the Italian Peninsula and the Island of Sicily and it connects the Ionian Sea, in the south side, and the Tyrrhenian Sea, in the north side, through a narrow and shallow gateway. Its morphology is shaped like a channel, meridionally oriented in the

southern and central part, bended eastwards in the northern part, and with a shallow sill in the middle part, that features its bathymetry.

Early surveys by Vercelli (1925), Defant (1940, 1961) and the University of Rome (Sapia et al. 1987; Di Sarra et al. 1987) gave explanation of the observed dynamics within the SoM, whose oceanographic features were comprehensively described by Bignami and Salusti (1990), laying the groundwork for further researches.

For what concern purely experimental studies a synthesis of Defant's analyses explain that the formation of barotropic tides in the SoM is mainly driven by the M2-tide that is playing a leading role in determining the general scheme of the current system. In the narrowest part of the Strait is located an amphidromic point and the phase of tidal velocity is seen changing by 180° within the width of the SoM, there, about 3 km. The tidal elevations are out-of-phase between the Tyrrhenian and Ionian Seas and related tidal velocities may increase up to 2-3 m/s. The tidal circulation is characterized by cyclonic and anticyclonic eddies that are located near Scylla, Punta Faro and Messina.

Later, in situ observations (e.g. Sapia et al. 1987; Di Sarra et al. 1987), and model applications (Del Ricco, 1982 Hopkinns et al, 1984), gave evidence that internal tides are also generated at the SoM, as similarly happens at the Strait of Gibraltar (Sánchez-Garrido et al. 2011). Synthetic aperture radar (SAR) images allowed identifying the origin and propagation of the internal solution (e.g. Alpers et al. 1983) and Brand et al. (1997) combined SAR images and a two-layer numerical model to describe its generation mechanism and propagation.

Model studies of the SoM were also proposed by Androsov et al. (2002a, 2002b) who used, first, viscous shallow-water equations to provide a synoptic description of the barotropic tidal dynamics and, then, three-dimensional equations to describe the variability of the density field. These authors focused their work on the spectral analysis of the sea surface solutions, detection of gyres and computation of the eulerian tide-induced residual current. The latter, a steady flow with time scale larger than a tidal period, is often used as indicator of the long term water exchange and transport on semi-enclosed basins, shallows and sea straits (e.g. Xuan et al., 2015).

The non-hydrostatic implementation of ocean numerical models found a natural application in straits where strong flows or density interfaces interact with rigid boundaries, as happen in the SoM. Sannino et al. (2013), for instance, adopted the non-hydrostatic version of the finite volume MIT-General Circulation Model (Marshall et al. 1997) in order to assess the energetic tidal potential in the SoM and they stirred up the adoption of similar tools to provide new insights into the nonlinear processes of the SoM dynamics.

In this paper, Fluidity-ICOM was applied in the SoM domain to provide a model investigation of the barotropic tidal dynamics, flows and residual complements. The domain of integration was discretized by a high-resolution unstructured grid that provided a refined representation of coastlines and bottom topography in the inner parts of the SoM and the whole domain. The model configuration can be found in Quattrocchi et al. (2016) where the same model case study has undergone a calibration procedure, in which the solution was compared with available observations and similar model approaches, with the aim of finding suitable parameterization and realistic output.

In the following, a synthesis of numerics, description of the domain of investigation, and the ocean model configuration is addressed (Section Numerical Model). In Section Results, the outcomes of the models are used to analyze the main features of the barotropic tide induced circulation along the SoM and their interaction with geometrical constraints. Conclusions, drawn by results, remind how barotropic tidal dynamics is significantly able to generate a wide spectrum of phenomena whose oceanographic implication, in more comprehensive model experiments, can be further investigated.

2. Numerical Model

Fluidity-ICOM solves the incompressible, non-hydrostatic Navier-Stokes equations in the Boussinesq approximation to describe the oceanographic physical model. These equations are discretized in a three-dimensional space defined by mean of an unstructured finite-elements computational mesh. Although, the model is also able to manage the adaptive re-meshing technology (Piggott et al. 2009), a static mesh was considered for the present model experiment.

The equation system is given by

$$\frac{\partial u}{\partial t} + \nabla \cdot uu + 2\Omega \times u = -\nabla p - \rho g k + \nabla \cdot \tau \quad (1)$$

$$\nabla \cdot u = 0 \quad (2)$$

where in the momentum equation (1) and continuity equation (2) u represents the three-dimensional velocity, Ω is the rotation vector and the earth spin effect is specifically computed at each latitude of the model domain. In these equations the part of the pressure term due to the weight of the fluid of reference density is balanced by the part of the gravity term that include the reference density and it is removed from the computation. The perturbation pressure p is instead computed and it includes the hydrostatic pressure, due to the perturbation density ρ, and the non-hydrostatic part of the pressure; k = (0,0,1) is the vertical normal vector. However for the present experiment only the reference density was declared and density variations were not considered (declared or computed). The viscous terms are represented by the stress terms τ that are related to the deformation rate tensor S_{ij} through the relation

$$\tau_{ij} = 2\mu_{ij} S_{ij} \quad (3)$$

where μ_{ij} is a diagonal matrix of viscosity, with horizontal (μ_{11} and μ_{22}) and vertical viscosities (μ_{33}), described by constant values. Imposing known initial and boundaries conditions at the model domain closes the system.
Beyond this concise and essential introduction on the numerical formulation in Fluidity-ICOM, the reader is addressed to Ford et al. (2004a, 2004b) for a complete and exhaustive description of all the numerical treatments.

2.1 Domain of integration

The model domain is located in the central part of the Mediterranean Sea and it focuses on the SoM and the surrounding area, within the overlaid red circle in Figure 1, left panel. The domain of integration includes relatively wide areas of the adjacent Tyrrhenian and Ionian Seas, allowing for a natural propagation of the boundary conditions through it. The right panel in Figure 1 displays the unstructured mesh adopted to discretize the model domain by mean of finite elements, which size varies between 2000 meters, at open boundaries, and 50 meters in the inner part of the SoM. In the same figure the colours of the mesh indicate the spatial variability of the high-resolution bathymetry that is derived by integration of GEBCO dataset (30 arc-second resolution) and nautical charts. The bathymetry of the model domain relevantly varies from the open boundaries to the inner part of the SoM. At the south entrance of the SoM the sea floor is at 1200 meters depth and it decreases up to reach the minimum value of 85 meters in the narrowest part, then, it increases again, up to 300 meters, towards the north entrance and the Tyrrhenian Sea. The meridionally oriented magnification of Figure 2 displays how a shallow sill divides a deep canyon, in the south, from a more gentle tilt in the north.

As complex as the bathymetry, the coastline shows relevant variations along both dimensions of a rather limited domain (Figure 2). From the south to the north part, the width of the SoM varies between 16.8 km (at the latitude of 38.016° N; south entrance) and 3.2 km in the narrowest part (between the latitudes of 38.231° N and 38.259° N, in vicinity of Punta Pezzo and Ganzirri, respectively), and it remains almost unvaried up to expand to the Tyrrhenian Sea. The SoM is shaped like a channel that is meridionally oriented in the southern and central part and bended eastwards in the northern part. The coastline of the model domain also describes the breakwaters in the port of Reggio Calabria, Villa San Giovanni and Scylla as well as the wider creek of Messina and the sharpened Punta Faro.

Figure 2 shows the geographical references of Scylla, Punta Pezzo, Villa San Giovanni, Reggio Calabria, Messina, Ganzirri and Punta Faro. The analysed temporal series refer to points that are located off of these locations. The white dashed lines define the cross sections (#1-#2 and #3-#4) along which the tidal flow will be considered in order to analyse the model solution.

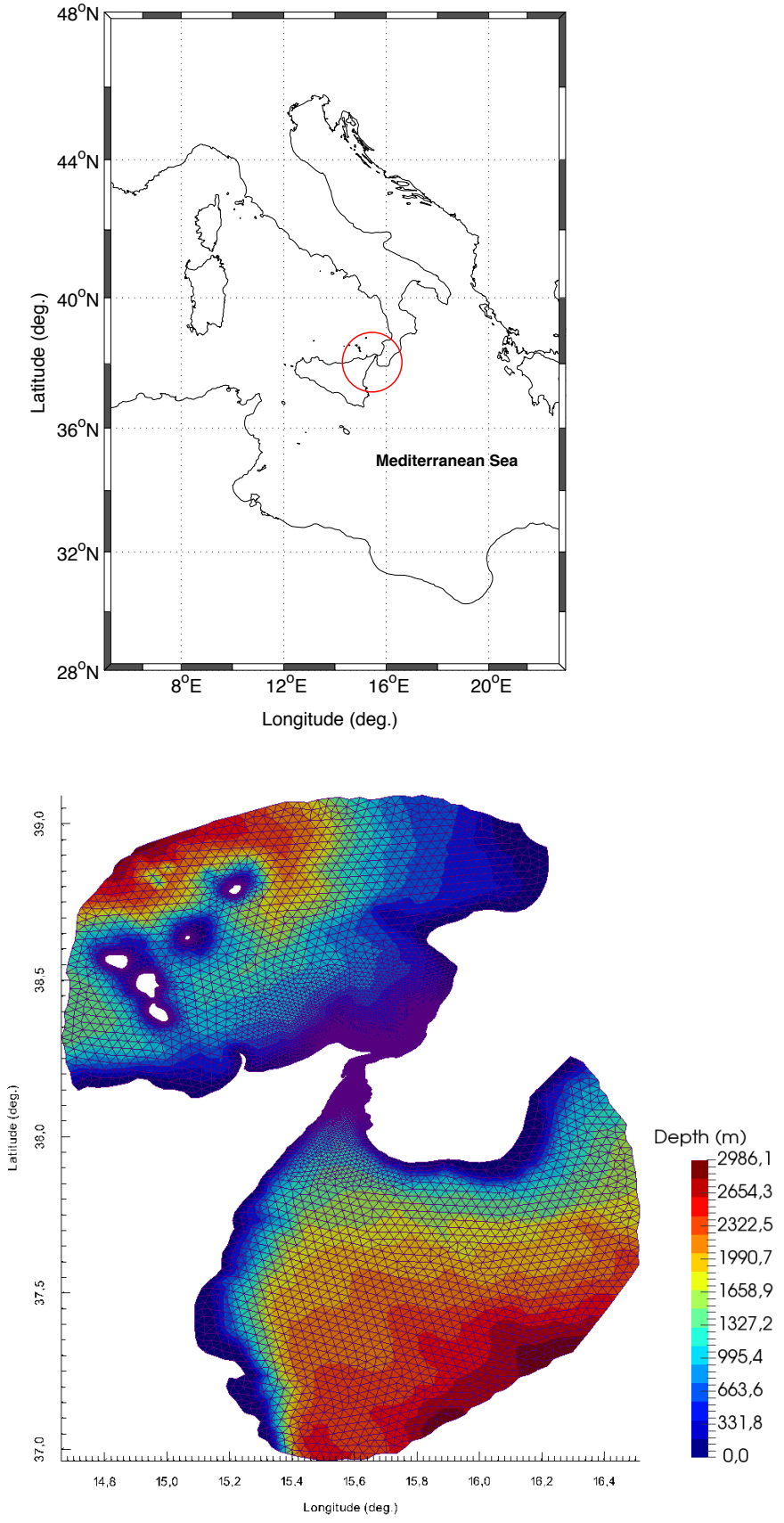

Figure 1: *Top panel:* Geographical references of the investigation area that is located in the Mediterranean Sea; the red circle defines the boundaries of the model domain. *Bottom panel:* Computational grid over bottom topography features (m).

2.2 Model configuration and boundary conditions

The model configuration is the same adopted in Quattrocchi et al. 2016. There, the model has undergone a calibration procedure during which the solution was compared with available observations and similar model approaches with the aim of finding suitable parameterization for the values of the bottom drag coefficient and the horizontal viscosities. Some relevant aspects of the model configuration are reported in the following.

Three-dimensional equations (1 and 2) that are discretized by mean of the finite element method describe the hydrodynamic system. Velocity and Pressure fields are discretized within a first-order continuous function space (known as P1-P1 finite element pair) and a stabilization term to the pressure equation is considered to avoid spurious pressure modes (Ford et al., 2004). The water column is discretized by mean of sixteen, equidistant sigma-layers where the nodes of the mesh are aligned vertically. With this vertical discretization the thickness of the deeper layer is varying between 75, in the deepest canyon, and 5 meters in the shallow part of the SoM.

The ocean problem is implemented on a spherical earth where the gravity points toward the centre of the sphere. The integration in time is provided by an implicit scheme that is unconditionally stable and allows for variable time step. The initial viscous terms, that represent the horizontal and vertical diffusion of momentum, were chosen as follow: $\mu_{11} = \mu_{22} = 200\ \mathrm{m^2 \cdot s^{-1}}$ and $\mu_{33} = 10^{-6}\ \mathrm{m^2 \cdot s^{-1}}$. Large Eddies Simulation model (Pope, 2000) with a second order closure scheme (Smagorinsky, 1963) was used to compute viscous terms during the integration time.

Closed boundaries conditions are characterized by a non-dimensional drag coefficient at the bottom with constant value of $C_{D\,bottom} = 2.6 \times 10^{-3}$ and a prescribed no–normal flow at the lateral boundaries. A tidal signal, for this experiment composed of the four more relevant diurnal (O1 and K1) and semidiurnal (M2 and S2) constituents, was prescribed at the open boundaries of the domain of integration through setting a Dirichelet condition at the non-hydrostatic part of the pressure. Tides are forced as cosine waves of specified phases and amplitude, derived by the Oregon State University dataset, that uses a model of the Mediterranean and Black Seas at 1/30° resolution, with eight main tidal constituents at open boundaries and assimilation from altimetry and in situ data (http://volkov.oce.orst.edu/tides/). Tidal potential is not considered due to the relatively limited extension of the domain of integration.

No stress conditions are applied at the free surface that can be excluded from explicit computation. However, its value can be diagnostically derived at each node by the pressure boundary condition $p = \rho g \eta$, perturbation density, gravity and free surface elevation, respectively.

Initial values for the three-dimensional velocity field and the scalar pressure fields are set to zero. The starting time of integration is set to zero and the simulation proceed up to 42 days with variable time step within the range of 20 and 100 seconds. The hourly output of surface elevation and velocity components was considered for analysis after four semidiurnal periods to avoid initial transients.

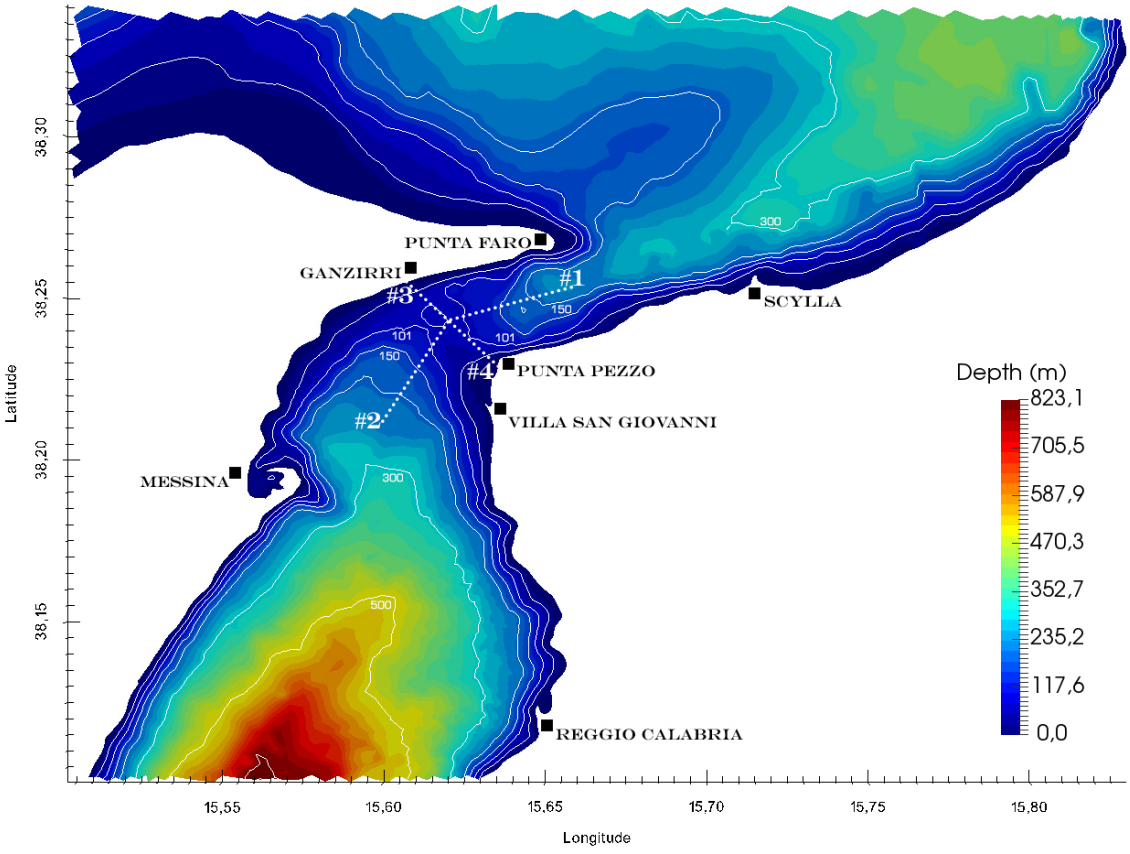

Figure 2: A magnification of the model domain that describe the complex nature of coasts and bottom topography of the Strait of Messina. The picture also describes the reference locations along the coasts and segments along which cross-sections are considered.

3. Results

In the following, the barotropic tidal dynamics of the SoM is explored through the solutions of this implementation of Fluidity-ICOM. The spectral analysis of the modelled sea surface, at specific locations of the domain of integration, displays the contribution of the main tidal constituents and co-oscillation tides in shaping the tidal dynamics. Maps and cross-sections of tidal flows provide information of the transient tidal-induced circulation at syzygy as well as tide-induced residual circulation, which arises from interaction between tidal flows and the geomorphology of the model domain.

3.1 Constraints of complex geometries

As early found by Defant (1967) and more recently described by Andersen (1999), the barotropic tidal dynamic in the SoM is mainly dominated by the M2-tide that also determines the general scheme of currents. Tidal maps of the M2-tide amplitude and its propagation in the SoM can be found in Quattrocchi et al. (2016).

Principal tidal constituents as M2-tide that propagate in shallow waters, and in this case between the Tyrrhenian and Ionian Seas into the SoM, become distorted and asymmetric due to complex coastal constraints and sea-floor friction that induce flow curvature effects (Defant 1961; Pugh 1987). These phenomena manifest themselves through the generation of co-oscillating tides, harmonic constituents with angular speed that is multiple (overtides), sum or difference (compound tide) of the angular speed of the main tidal harmonic constituents. Overtides and compound tides that appear in the tidal spectra arise from the interaction between different fundamental frequencies and sea-floor

morphology (Andersen 1999; Quattrocchi et al. 2016). Known as shallow water tides (Le Provost, 1981), they are one of the most evident nonlinear physical processes in many coastal areas, where they produce flood/ebb asymmetries and strongly affect the long-term distribution of sediments (Friedrichs and Aubrey, 1988).

In the SoM, the south entrance is more then 5 times wider than the north entrance and the deepest canyon of the sea floor is more than 10 times deeper than the shallow sill in the central part. These ratios indicate the complex nature of the coastal constraints where tides propagate, in the SoM, promoting distortions and nonlinear growth of overtones and compounds constituents.

In this model case study, two diurnal and two semidiurnal tidal constituents drive the solution of Fluidity-ICOM and the spectral analysis (Pawlowicz et al. 2002) was used to extract tidal constituents from three, 40-days long time series of the modelled sea surface. The time series were relieved in proximity of three locations along the model domain representing the SoM (see Figure 2): offshore Scylla, located at the north entrance of the SoM, offshore Punta Pezzo, over the sill and out the harbour of Reggio Calabria, located at the south entrance of the SoM.

At Reggio Calabria all the main constituents (M2, S2, K1, O1) that were provided at open boundaries of the model domain appear in the spectrum (Figure 3, top panel). Diurnal and semidiurnal tidal constituents shade overtones and compound harmonics whose amplitudes do not exceed few millimetres. Punta Pezzo (Figure 3, middle panel) is located over the sill, in the narrowest part of the SoM. There, the amplitude of overtides and compound tides increase due to the nonlinear distortions of the major astronomical tidal constituents in shallow water and the spectrum became more flat. Overtones increase their amplitude up to 5 centimetres, as found for M4-tide, and sixth- and eight-diurnal frequencies, like M6 and M8 tidal constituents also appear in the spectrum. In the same spectrum, the amplitude of compound tides MK3, SK3 and MS4 is also noticeable. Off Scylla (Figure 3, bottom panel), only the main tidal constituents have significant amplitudes, as found for Reggio Calabria, and limited amplitudes of composite tides.

As similarly found by Androsov et al., (2002), the spectra in Figure 3 reveal important differences along the east edge of the SoM. The semi-diurnal lunar tide M2 is the dominant astronomical constituent that appears with maximum values in the spectra at both entrances of the SoM (Scylla and Reggio Calabria) and M4 is the most significant overtide. M4 to M2 amplitudes ratio can be considered as a direct measure of non-linear distortion of barotropic tides in the SoM; the larger the M4/M2 ratio, the more distorted the tide becomes (Friedrichs 1988). This behaviour is marked by the spectra in Figure 3 where the amplitude ratio is near to zero at Reggio Calabria (the south wide entrance of the SoM), it increases to 0.13 at Scylla (the north narrow entrance of the SoM) and it becomes greater than one at Punta Pezzo, where the considerable coastal constraint and a shallow sill profoundly distort this modelled barotropic tidal signal.

The high gradient of the sea-floor morphology, featuring the SoM, and the considerable reduction of the width from entrances to the central part is hence able to distort tides and modify intensities and directions of flood and ebb velocities and it generates nonlinear behaviours due to friction at the sea-floor and spatial advection. As will be shown with maps of the tidal currents, the barotropic tidal currents that are flowing through the SoM, from Tyrrhenian to Ionian Seas and vice versa, increase their intensity according to Bernoulli effect, hence, to the width and sea-floor depth that define the dimension of the flow section.

The behaviour of tidal currents in the inner part of the SoM is displayed in Figure 4 by mean of two temporal series of the modelled surface velocity. These series refer to the current speed at two points located in the sill region, where the highest tidal velocities are found. The couple is located off Ganzirri, in proximity of the west edges (Figure 4, top panel) and off Punta Pezzo, in proximity of the east edges (Figure 4, bottom panel). Maximal velocities at these locations reach the values of 2.2 and 1.8 m/s, respectively. Both signals display the same periodicity and by including more than a synodic month they describe the tidal velocity related to spring and neap tides. During both, syzygy and quadrature, diurnal maxima and maxima with six-hour frequency are indistinctly found in these series. A comparison between them suggests that maxima display the same values during quadrature but different values during syzygy. The difference, about 0.4 m/s, is a considerable value that quantifies the zonal gradient of the tidal velocity field that is found over the sill. During syzygy, the effect of the sea-floor morphology of the sill, which is characterized by a wide shallow off Punta Pezzo, is able to amplify the flow speed.

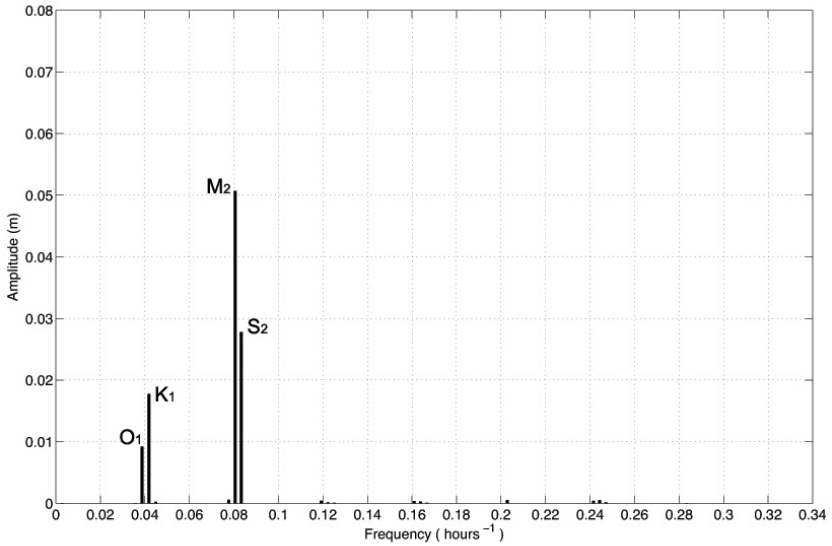
Amplitude (m)
Frequency (hours $^{-1}$)
M2
S2
K1
O1

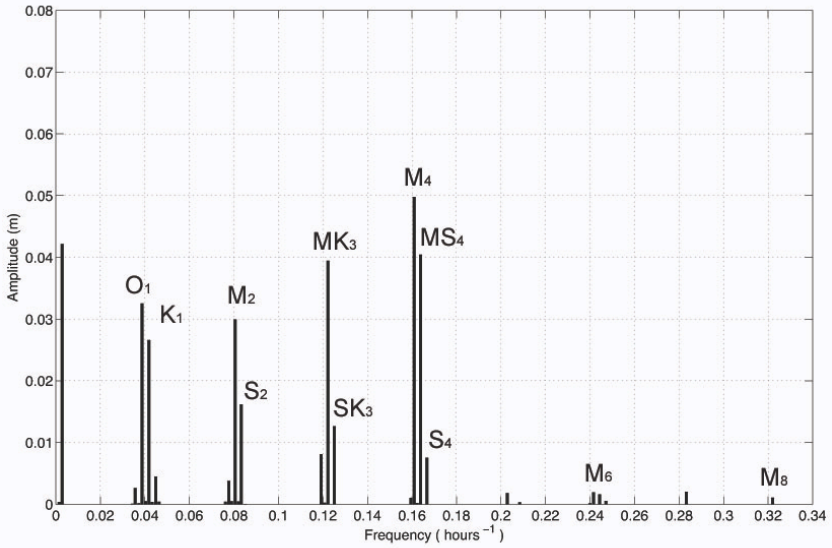
Amplitude (m)
Frequency (hours $^{-1}$)
M4
MS4
MK3
O1
K1
M2
S2
SK3
S4
M6
M8

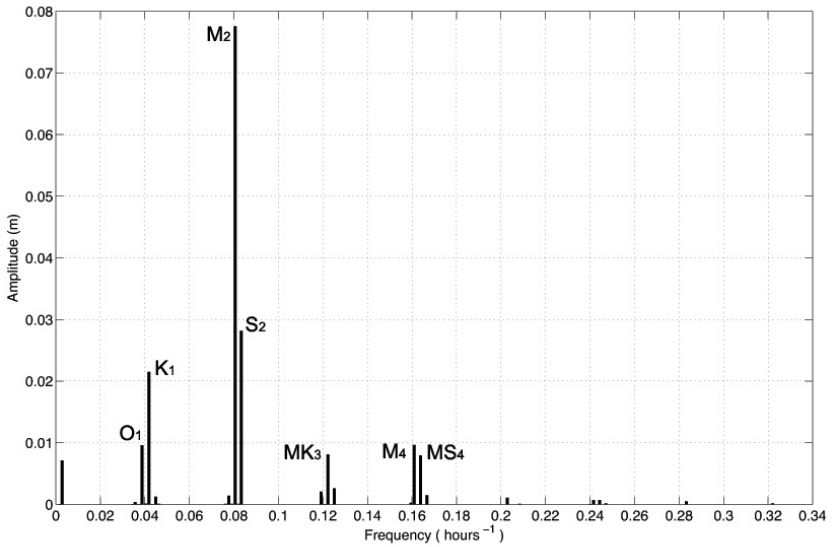
Amplitude (m)
Frequency (hours $^{-1}$)
M2
S2
K1
O1
MK3
M4
MS4

Figure 3: Spectra of the modelled sea surface height displaying the amplitudes (m) at three reference points along the coast of the Strait of Messina. *Top, middle and bottom panels* refer to Reggio Calabria, Punta Pezzo and Scylla, respectively.

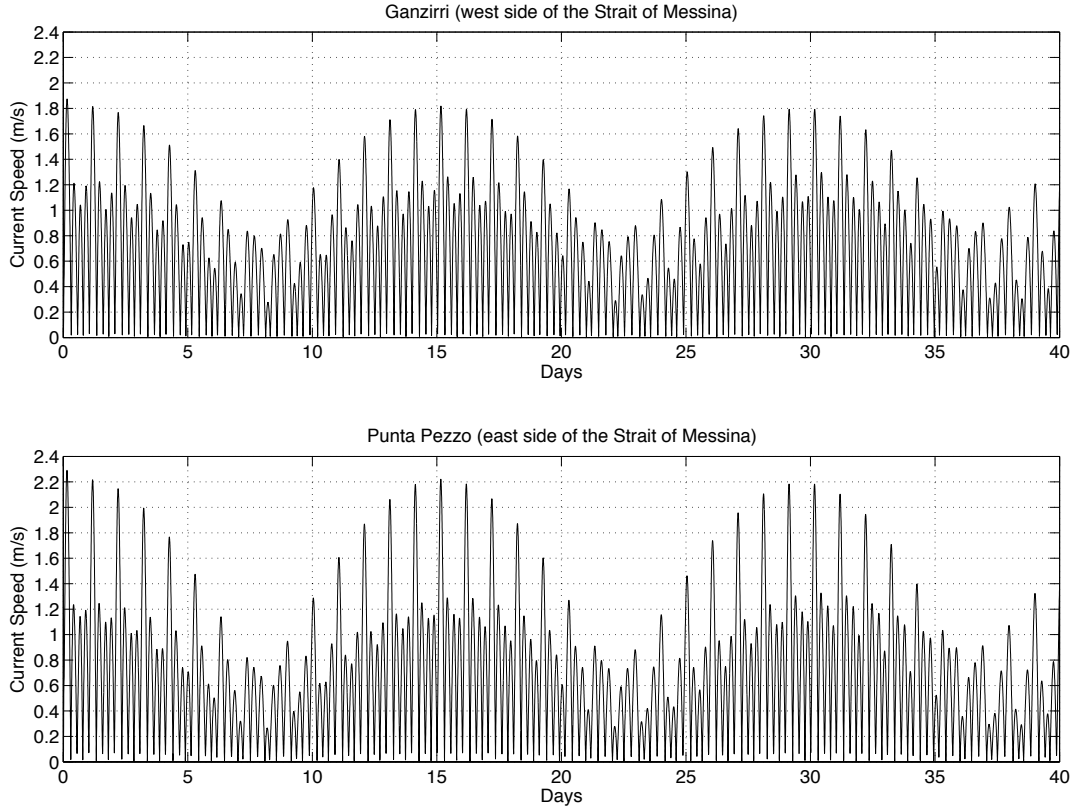

Figure 4: Temporal series of the modelled tidal flow speed (m/s) at the sea surface as relieved offshore the locations of Ganzirri (*top panel*) and Punta Pezzo (*bottom panel*).

3.2 Tidal Flows

The 41-days long temporal series in Figure 4 display the behaviours of the barotropic tidal flow in the inner part of the SoM during more than a synodic month. Moreover, synoptic maps of the tidal flows, related to specific instances of such integration time, point up how flood and ebb conditions are able to generate northward and southward flows in the SoM, and how they promote transient recirculations.

In the following, maximal of tidal northern and southern flows, for spring tides are discussed by analyzing colour maps of the simulated sea surface height (hereafter SSH) with overlapped tidal flow vectors. Moreover, cross-sections display the behaviour of the three-dimensional velocity, as computed by the non-hydrostatic numeric implemented in Fluidity-ICOM, and it provides information about the vertical acceleration of the barotropic tidal flow while it is approaching or leaving the shallow area of the SoM. Cross-sections of the tidal flows were relieved along the segments, #1-#2 and #3-#4 (see Figure 2); meridional, zonal and vertical components of velocity are defined positive northward, eastward and upward, respectively, and they were projected along or across each sections.

The instance of maximal northward tidal flow is displayed in Figure 5. This map displays a SSH of 0.08 m, at south and -0.12 m at the north side of the SoM, with a domain-scale maximum range of roughly 0.2 m. A limited area with the high negative values of -0.3 m, on average, is instead found in correspondence of the sill, off Punta Pezzo. Thus, when

the water is flowing toward north a gradient of 0.38 meters is found from the south entrance to the sill region of the SoM.

The tidal flow, related to this SSH gradient, is coming from the south side of the SoM, where it displays a speed of 0.2 m/s that increases up to reach the maximum value of 2.95 m/s, in correspondence of the wide submerged platform around the sill. Approaching the sill, the flow slightly changes in direction and displays a zonal negative gradient, between 2.8 and 1.3 m/s, from the east to the west edge. At the north side of the SoM, before to converge to the Tyrrhenian Sea, the flow mostly keep its speed and it is able to generate a recirculation north of Punta Faro and off Scylla, due to inertial mechanisms. Thus, the flow decreases to minima values of 0.2 m/s that are found offshore, out of the SoM.

A representation of the tidal flow behaviours along the meridional direction is given in Figure 6, top panel, where section 1-2 displays, with colours, the intensity of the vertical component of the tidal flow and, with arrows, the velocity components that are projected on the plane lying on the section. The computed vertical velocities reach values of 0.11 m/s in both, upward (red) and downward (blue) directions; the sign inversion is represented by white contours. Maximum values are found in proximity of the sill, before it and immediately after it, emphasizing the effect that the bottom topography has on the tidal flow behaviour. These effects are also found far from the sill, associated to smallest seabed changes. Beside, the intensity of the projected, along section, tidal flow is much stronger, displaying maxima of 2.14 m/s when it moves toward north from point #2 to point #1of this section.

In Figure 6, bottom panel, the horizontal components of the tidal flow are projected along the normal to the section #3-#4; their intensity is displayed with colours and the advection direction with the overlaid arrow. An intense core of 2.88 m/s is found in the eastern part of the section where the water depth decreases as approaching to the coast. The overlapped arrows represent the vertical component of the three-dimensional velocity vector that in this case displays a strong downward velocity at the east part of the section with maxima of 0.18 m/s and weaker upward vertical flow at the west part.

The instance of maximal southward barotropic tidal flow is given in Figure 7. This map displays a SSH of +0.13 m, at north and -0.07 m at the south side of the SoM, with a domain-scale maximum range of roughly 0.2 m. A limited area of high negative value of -0.16 m, on average, is instead found in correspondence of the sill, off Punta Pezzo. Thus, when the water is flowing toward south a gradient of 0.29 m is found from the north to the sill region of the SoM.

From the north to the south side of the SoM the flow speed is almost uniform except in correspondence of the central area, where maximum velocity magnitude of 2.2 m/s is found. The flow approaching the central area, corresponding to the sill of the SoM, amplifies its speed and slightly changes the direction, following the west edge of the SoM. A zonal positive gradient, from the east to the west edge, is only found south of the sill. Transient recirculations are not strong and they are found south of Punta Pezzo with moderate speed of 0.2 m/s.

Sections #1-#2 and #3-#4 in Figure 8, top and bottom panels provide a clear representation of the southward tidal flow behaviours along the water column. Reference arrows indicate that this instance of the tidal flow is less intense than the northward counterpart. In section #1-#2 maxima of 1.65 m/s are found in proximity of the sill and the vertical component of the tidal flow, described with colours, is more intense at north, where the flow is approaching the sill in the narrowest part of the strait, and less intense at south where the strait starts to opening toward the Ionian Sea. In section #3-#4 the maximum flow normal to the section is found within a core near 1.9 m/s. At the east and west boundaries, the flow is weaker with minima of 0.2 m/s. The vertical component of the velocity vector is stronger in correspondence of the core of the meridional flow, with maxima of 0.13 m/s and upward direction.

These key barotropic tidal flow features, given by interpretation of the above presented model solution, agree with observational counterparts and model experiments; for instance, the measurements of Mosetti (1988) provided estimates of the maximum velocity of the summary tidal currents for 14 harmonics in 2.895 m/s, and more recent punctual measurements and numerical model solutions (Sannino et al. 2013, 2015; Androsov 2002a, 2002b) also endorse the above presented results, reminding the relevance of the barotropic dynamics.

However, if addressed, modern and ad-hoc designed experimental surveys would give improved comprehension of the three-dimensional tidal flows dynamics and would provide calibration and validation of this barotropic, and a further

baroclinic implementation of Fluidity-ICOM. Indeed, ocean modelling could more satisfactorily represent the dynamics in straits and critical areas.

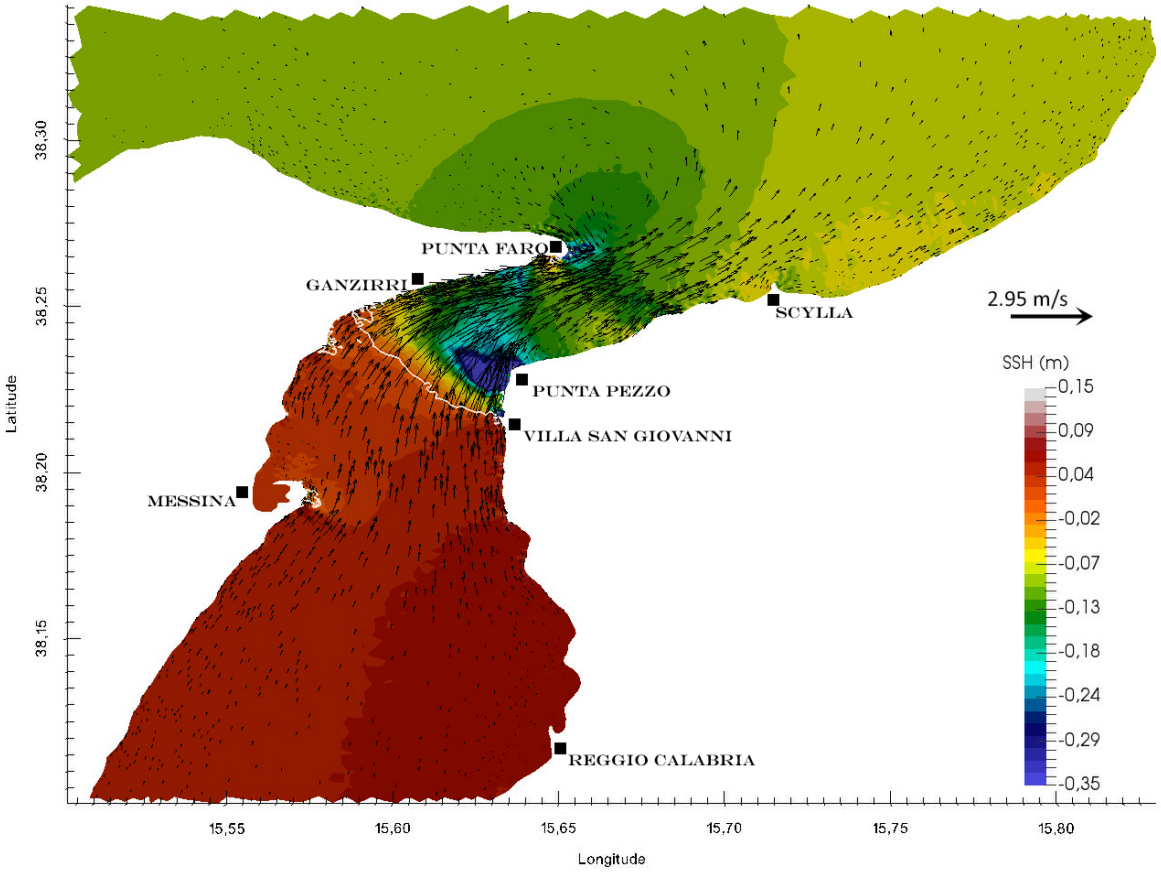

Figure 5: Snapshot of the instance of maximal northward barotropic tidal flow (m/s) during syzygy. The map is showing the modelled sea surface height displacement (m) overlapped by black arrows scaled by intensity. White contours define the zero sea surface displacement.

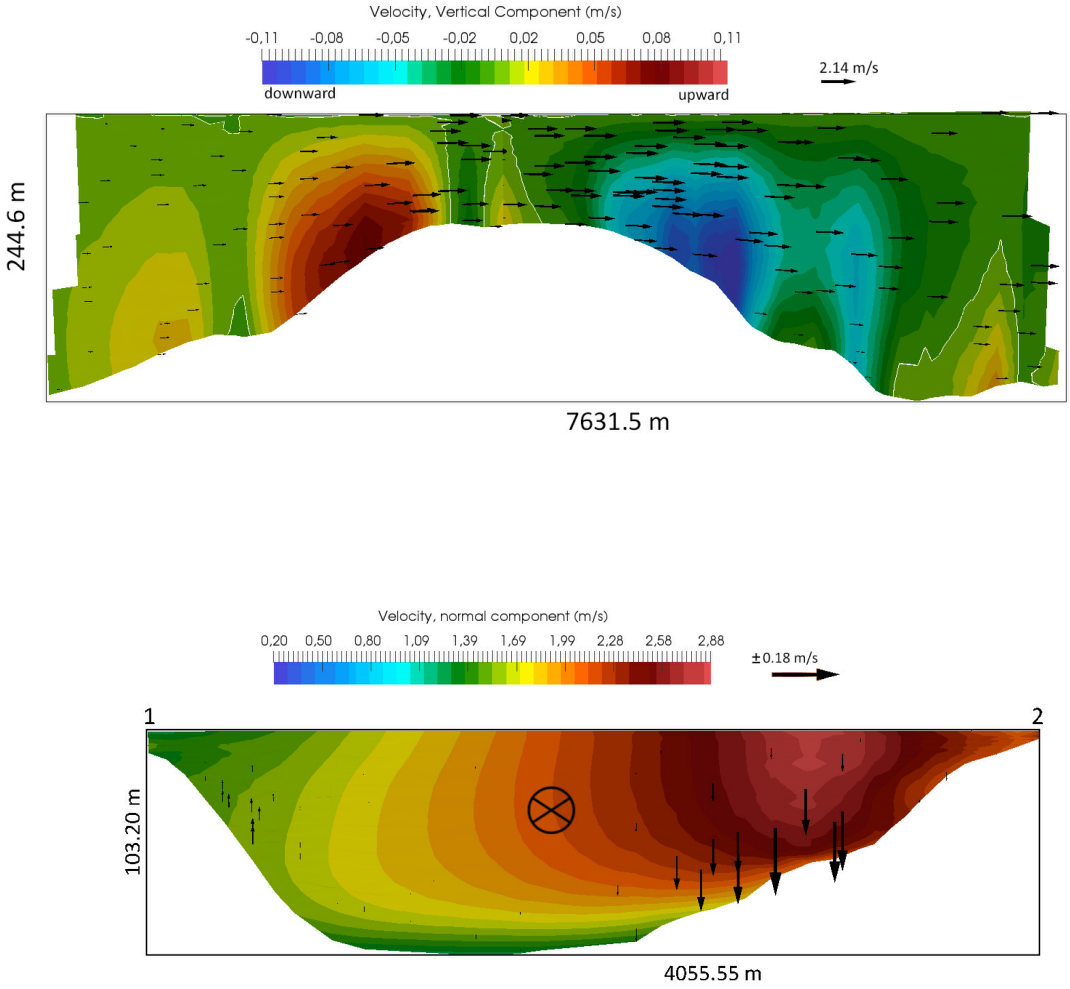

Figure 6: *Top Panel:* Cross-section, along the segment 3-4, of the maximal northward barotropic tidal flow; the colours indicate the intensity of the horizontal components of the velocity vectors (m/s), normal to the section; the overlapped notation for vectors in of the plane gives the direction of the normal vector; the overlapped arrows, scaled by intensity, refer to the vertical component of velocity (m/s) lying on the plane, positive upward and negative downward. *Bottom panel:* Cross-section, along the segment 1-2, of the maximal northward barotropic tidal flow; the colours indicate the intensity of the vertical component of the velocity vectors (m/s), positive upward and negative downward; the white contours indicate zero vertical velocity; the overlapped black arrows, lying on the plane and scaled by intensity, refer to the velocity vectors (m/s) that are projected along the plane.

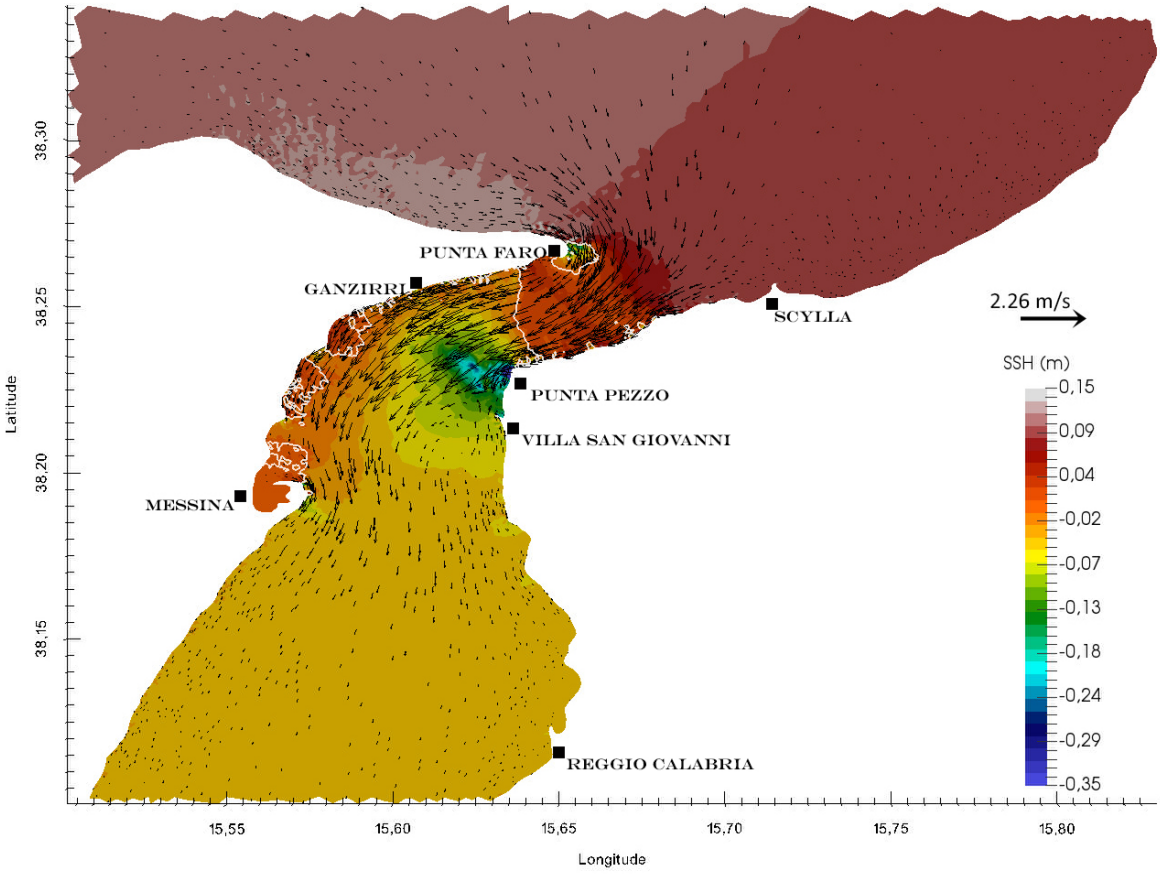

Figure 7: Snapshot of the instance of maximal southward barotropic tidal flow (m/s) during syzygy. The map is showing the modelled sea surface height displacement (m) overlapped by black arrows scaled by intensity. White contours define the zero sea surface displacement.

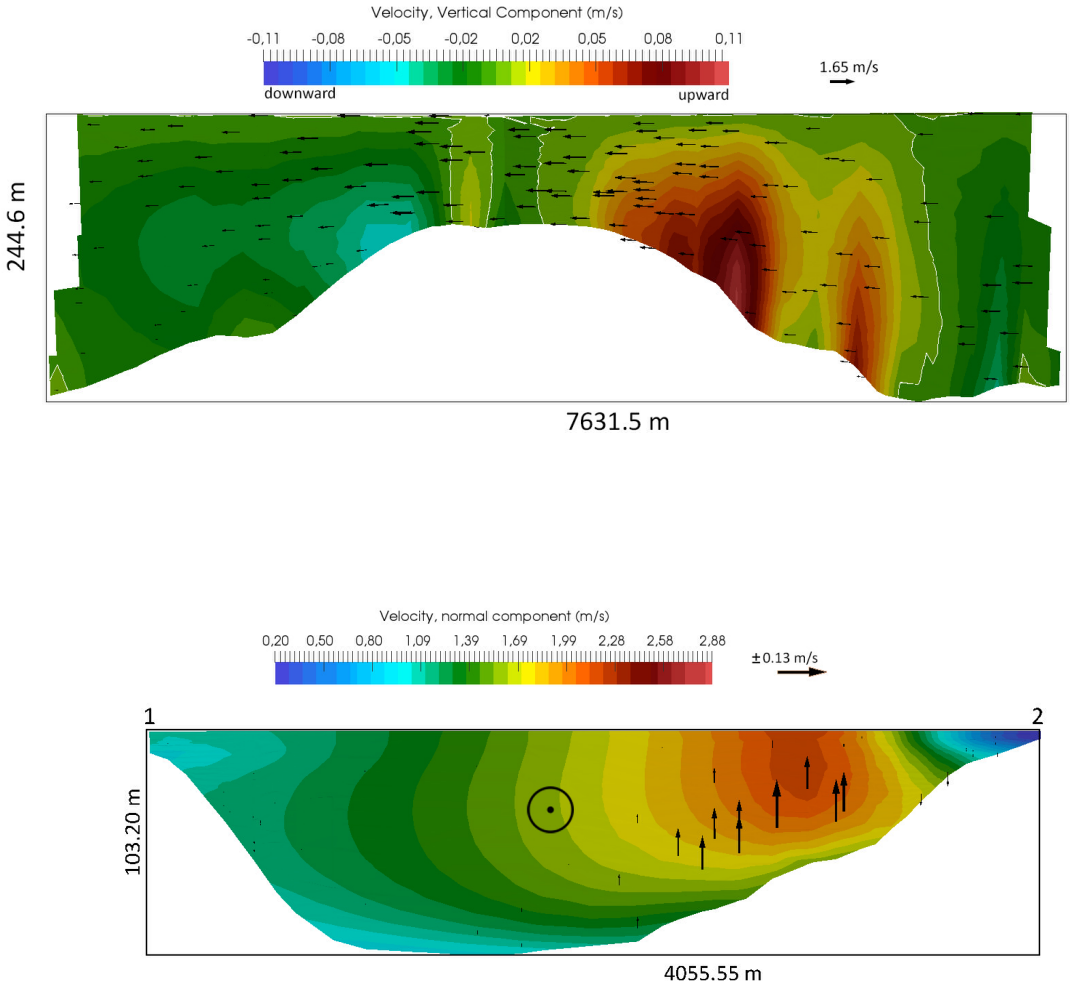

Figure 8: *Top Panel:* Cross-section, along the segment 3-4, of the maximal northward barotropic tidal flow; the colours indicate the intensity of the horizontal components of the velocity vectors, normal to the section (m/s); the overlapped notation for vectors out of the plane gives the direction of the normal vector; the overlapped arrows, scaled by intensity, refer to the vertical component of velocity (m/s) lying on the plane, positive upward and negative downward. *Bottom panel:* Cross-section, along the segment 1-2, of the maximal southward barotropic tidal flow; the colours indicate the intensity of the vertical component of the velocity vectors, positive upward and negative downward (m/s); the white contours indicate zero vertical velocity; the overlapped black arrows, lying on the plane and scaled by intensity, refer to the velocity vectors (m/s) that are projected along the plane.

3.3 Gyres

The curl of the barotropic tidal flows provides indication of the vorticity fields in the SoM and it is computed according to the following equation

$$\text{curl}\,\mathbf{u} = \left(\frac{\partial w}{\partial y} - \frac{\partial v}{\partial z}\right)\mathbf{i} + \left(\frac{\partial u}{\partial z} - \frac{\partial w}{\partial x}\right)\mathbf{j} + \left(\frac{\partial v}{\partial x} - \frac{\partial u}{\partial y}\right)\mathbf{k}$$

where **u**(u, v, w) is the vector velocity field. Vorticity describes the rotation of the three-dimensional velocity vector, defining the circulation density of a moving flow that, in this case, may only arise by interactions between tidal flows

and geographic and topographic constraints. The horizontal vorticity field in the left panel (right panel) of Figure 9 correspond to the same instances of the tidal flow displayed in Figures 5 (7); the maximum northward flow and the maximum southward flow, during a spring tide.

During the northward instance the horizontal component of the circulation density displays its maxima in correspondence of the shallower part of the SoM, a wide submerged platform extending between Villa San Giovanni and Punta Pezzo. Off Ganzirri and Punta Faro the circulation density also reach maximum values due to inertial circulation associated to coastal constraints and bathymetric features. In the central part of the SoM high values provide indication that the northward flow is bending east as the coasts do. Significant values are also found north of Punta Pezzo along the east edge where the flow energetically meanders up to Scylla and off Messina where three limited areas of noticeable value of circulation density are found.

During the southward instance the circulation density reduces in correspondence of the shallower part of the SoM and off Ganzirri. Punta Faro still displays high values with patterns being shifted slightly northward. North of Punta Pezzo, along the east edge of the SoM, the circulation density is unvaried, while it disappears at Scylla. With respect to the northward instance, the patterns off Messina do not vary their position but slightly reduce their intensity.

The presence of gyres off Scylla, Punta Faro and Messina was early reported by Defant's theoretical schemes and model solutions of Androsov (2002a) also add Punta Pezzo between the main transient gyres in the SoM. The detailed representation of the above presented results give evidence that gyres can be also found off Villa San Giovanni and Ganzirri.

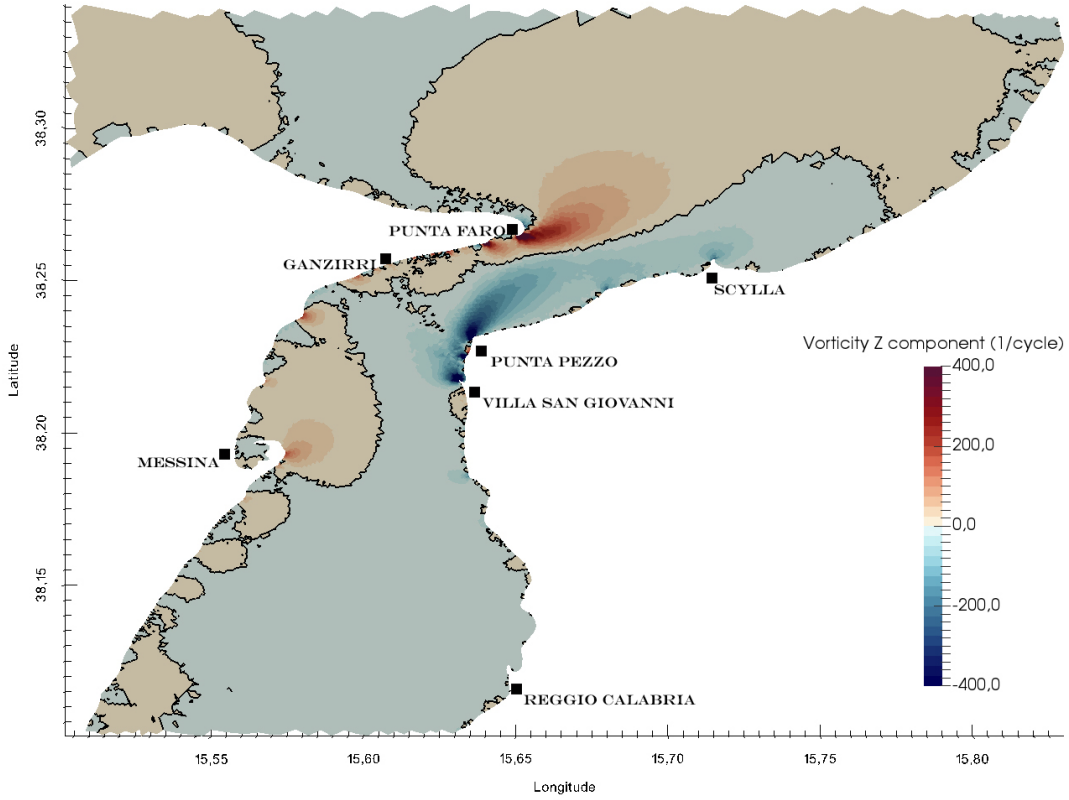

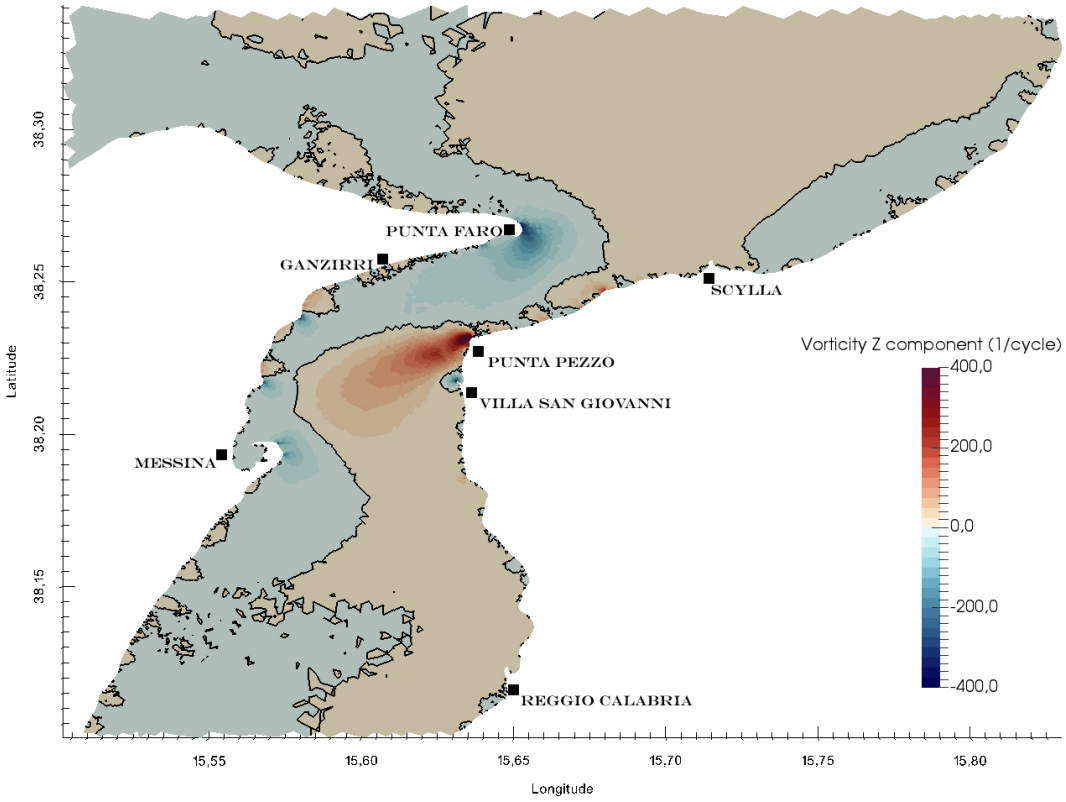

Figure 9: Snapshots of the horizontal component of the circulation density (c^{-1}). *Left and right panel*s refer to the instance of maximal northward and southward tidal flow, corresponding to Fig. 5 and 7. Positive values (in red) refer to an anticlockwise rotation; negative values (in blue) refer to a clockwise rotation.

3.4 Residual Circulation

In the SoM topographic obstructions as the central sill and areas of bottom topography shallows promote topographic tidal rectification. These nonlinear modifications of tidal flows may, in turn, generate transient secondary circulation around promontories or bottom complex features (Tee, 1977). Vorticity vector fields, computed for a specific time give an approximate representation of this transient secondary circulation that generally arise around capes, (e.g. Figure 9) and even sills and shallows, where it increases its rotational behaviour.

The computation of the Eulerian tide-induced Residual Current (hereafter ERC) provides a convenient way to display and interpret the main features of a secondary mean circulation and it is computed according to the following formulation

$$\mathbf{u}_e = \frac{1}{T}\int_0^T \mathbf{u}(t)\, dt$$

where **u** is the velocity vector, e stand for eulerian and T represents a characteristic period (Tee 1977; Imasato 1983, Robinson 1983). ERC is the result of a filtering method in which the velocity vectors are time-averaged to remove the tidal signal and it provides a depiction of a steady current that integrates the transient circulation within a characteristic timescale (T), longer than a tidal period. The results of this mathematical expedient are not the physical reality, but they provide an effective representation of the current system arising from the interaction between tidal forcing and physical constraints. This is especially true in the domain of the SoM where tidal effects are often sufficient to account for most of the dynamics.

Excluding the spin up period, Figure 10, top panel, displays the ERC at the surface, computed for the model domain within the integration time of 40 days, that includes a neap-spring variation. In this picture the colour map defines the

intensity of the residual current (maximum values is found to be 0.36 m/s) and the arrows, scaled by intensity, indicate its direction.

Offshore, at north and south parts of the SoM, the intensity of ERC is below 0.1 m/s. In proximity of the northern entrance of the SoM, the ERC displays a wide cyclonic recirculation with maximum values in correspondence of solid boundaries. By contrary, at the southern entrance, a strong cyclonic recirculation occupies the entire width of the SoM, between the coastal areas of Messina and Villa San Giovanni. In the narrowest part of the SoM, between the localities of Punta Pezzo, Punta Faro and Ganzirri the recirculation displays anticyclonic behaviour and maximum values are found at the west edge of the SoM.

Figure 10, bottom panel, displays section #5-#6 that is relieved in correspondence of the southern recirculation. This cross-section gives a depiction of the ERC three-dimensional structure. Colors represent the intensity of the ERC normal component, which advection direction is described with the overlapped black symbols. It ranges between zero (white contours) and 0.2 m/s and it is characterized by two opposite strong cores that are confined within the first 100 meters depth, the stronger is located at the east side and the weaker at the west side of the SoM. The behaviour of the computed vertical velocity component is described by mean of the overlapped, intensity scaled, black arrows. The vertical component is pointing toward the upward direction at the east side and toward the downward direction at the west side, indicating that the three-dimensional ERC is following the solid boundaries constraint with a non-negligible intensity close to 0.01 m/s. These results emphasize how, during the simulated synodic month, the effects of rigid constraints and consequent bottom/side friction emerge through the generation of fixed signs of vorticity of the ERC.

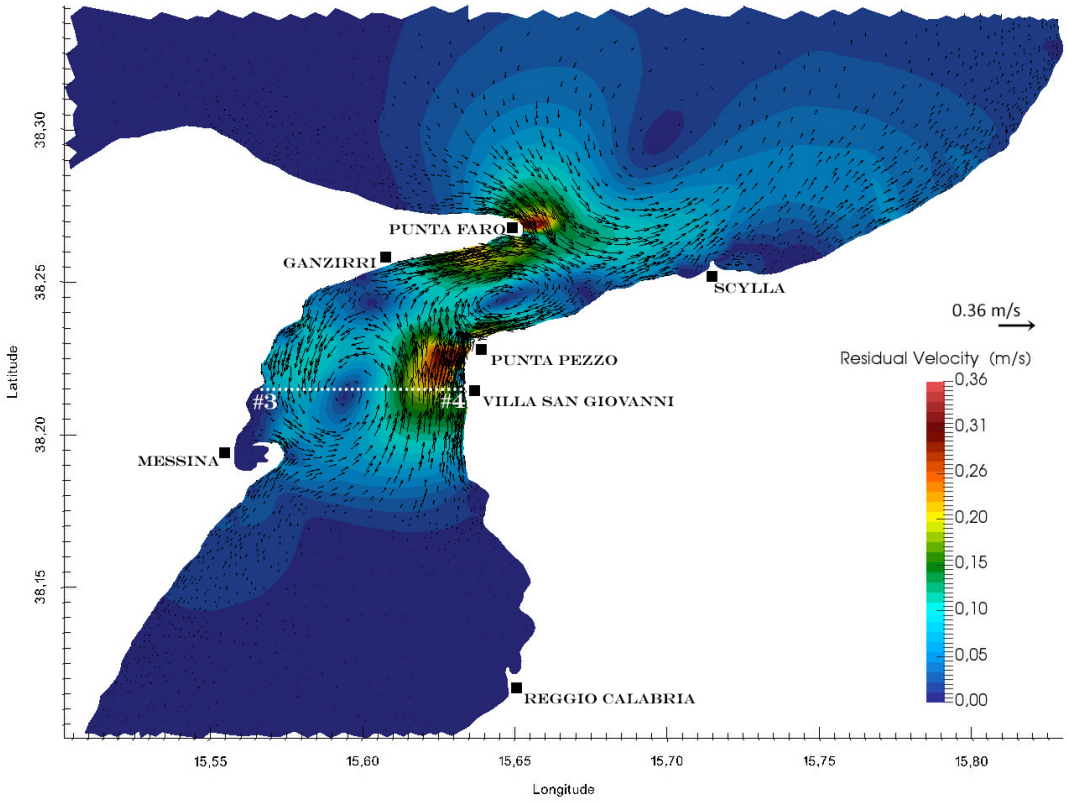

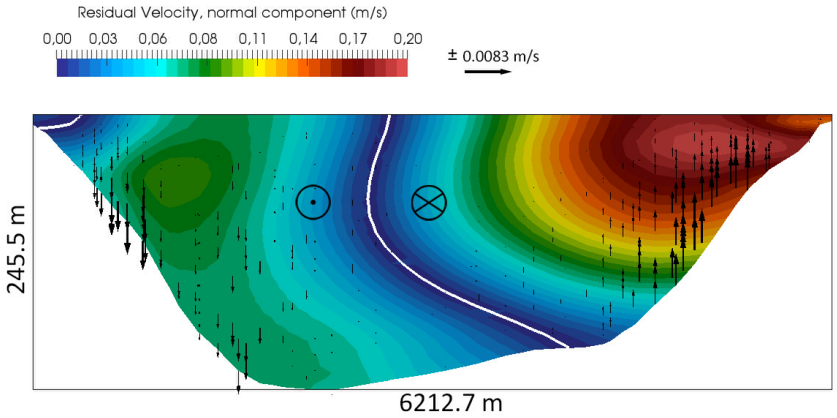

Figure 10: *Top panel:* Map of the horizontal components of the eulerian tide-induced residual circulation (ERC) at the sea surface (m/s); the colours indicate the current speed while overlapped black arrows indicate intensity (scaled by intensity) and direction. *Bottom panel*: Cross-section of the ERC along the segment 5-6; the colours indicate the intensity of the horizontal components of the velocity vector, normal to the section (m/s); the overlapped notation for vectors in and out of the plane gives the direction of the normal vector; the white contours indicate the zero normal velocity; the overlapped arrows, scaled by intensity, refer to the vertical component of velocity (m/s) lying on the plane, positive upward and negative downward.

4. Conclusions

In this paper a model study of the barotropic tidal dynamics is presented. The adoption of the ocean model Fluidity-ICOM has provided an inclusive investigation of flows and eulerian residual complements in the Strait of Messina (Italy). The latter is a sea strait of the Mediterranean basin experiencing a wide and fascinating range of observable natural phenomena. Fluidity-ICOM includes a number of features that make it a suitable investigative tool for this domain. Indeed, it solves the incompressible, non-hydrostatic Navier-Stokes equations that are discretized in a three-dimensional space defined by mean of an unstructured finite-elements computational grid, finding a natural application in straits where strong flows interact with rigid and convolute boundaries.

The adopted simplified model configuration purely includes a tidal signal that is prescribed at the open boundaries of the domain of integration as cosine waves of specified M2, S2, O1 and K1 amplitudes and phases. The main finding were partially described in Quattrocchi et al. (2016) and then, extensively tackled in this paper. Harmonic analysis of the simulated sea surface height elevation at specific locations along the meridionally oriented boundaries of the Strait of Messina have explained where the effects of geometrical constraints mainly promote the generation of overtides and compound tides. Temporal series and maps showed the main spatial and temporal behaviour of the simulated tidal flow whose intensity displayed its maxima in correspondence of the central part of the Strait of Messina, where its section significantly reduce in width and depth. Northward and southward oriented tidal flow was analysed at the surface and along specific cross-sections, showing a nearly uniform strong flow along the water column, with maxima during the northward instance. The main features of the vertical component of the simulated tidal flow were interpreted with cross-sections, which emphasized the direct effect of boundaries constraints on the vertical acceleration.

Further post-processing gave evidence that transient recirculation relevantly occur along the domain of investigation as showed by maps of the horizontal component of the vorticity, derived by surface instantaneous northward and southward oriented tidal flows. Filtering out the strong tidal signal the eulerian tide-induced residual circulation offers a

convenient interpretation of the main features of a secondary stationary circulation that is promoted by the interaction between tidal forcing and boundaries constraints.

As explained in the results section, these model outcomes, that were mainly expected, due to the simplified approach and model configuration, remarkably endorse previous model study results. The present investigation also highlights how, at sea straits, the knowledge and awareness of the barotropic tide-induced phenomena can be important when a more comprehensive oceanographic investigation is addressed. For instance, such a pronounced spring-neap cycle is able to increase the time-averaged benthic stress enhancing tidal mixing over the sill.

Literature indicates that a number of major questions concerning the oceanography of the Strait of Messina need to be further investigated. For instance, the propagation of internal waves and their potential braking over sloping topography as well as, citing an example of contemporary issues, the local small scale processes where the role of the turbulence is prominent and by which it could be possible to analyse horizontal and vertical, transient vortices.

An advanced baroclinic implementation of Fluidity-ICOM could be able to provide a useful approach to tackle these open problems in the domain of the Strait of Messina. Thus, whether a modern and ad-hoc designed experimental survey could accompany the model hypotheses, basin scale ocean modelling could benefit from a more accurate knowledge of significant phenomena that occurs at sea straits and other critical transitional areas.

Acknowledgement

I would thank the Applied Modelling and Computation Group (AMCG) of the Imperial College of London for valuable support.

References

Alpers,W. and Salusti, E. 1983. Scylla and Charybdis observed from space. Journal of Geophysical Research 88(C3), 1800–1808, doi:10.1029/JC088iC03p01800.

Andersen, O. B. 1999. Shallow water tides in the northwest European shelf region from TOPEX/POSEIDON altimetry, Journal of Geophysical Research, 104(C4), 7729–7741, doi:10.1029/1998JC900112.

Androsov, A.A., Kagan, B.A., Romanenkov, D.A., Voltzinger, N.E., 2002a. Numerical modelling of barotropic tidal dynamics in the strait of Messina. Adv. Water Resour. 25, 401–415. doi:http://dx.doi.org/10.1016/S0309-1708(02)00007-6

Androsov, A.A., Voltzinger, N.E., Romanenkov, D.A., 2002b. Simulation of three-dimensional baroclinic tidal dynamics in the strait of Messina. Izv. - Atmos. Ocean Phys. 38, 105–118.

Battaglia M., Caserta A., Salusti E., 1995. Transient phenomena in the Strait of Messina. In the Strait of Messina Ecosystem, Guglielmo L., Manganaro A. and De Domenico E. Editori, 31-48.

Bignami, F. and Salusti, E. 1990. Tidal currents and transient phenomena in the Strait of Messina: A review. The Physical Oceanography of Sea Straits, L. J. Pratt, Ed., Kluwer Academic, 95–124.

Brandt, P., Rubino, A., Alpers, W., Backhaus, J.O., 1997. Internal Waves in the Strait of Messina Studied by a Numerical Model and Synthetic Aperture Radar Images from the ERS 1/2 Satellites. J. Phys. Oceanogr. 27, 648–663. doi:10.1175/1520-0485(1997)027<0648:IWITSO>2.0.CO;2

Cucco, A., Quattrocchi, G., Olita, A., Fazioli, L., Ribotti, A., Sinerchia, M., Tedesco, C., Sorgente, R., 2016. Hydrodynamic modeling of coastal seas: the role of tidal dynamics in the Messina Strait, Western Mediterranean Sea. Nat. Hazards Earth Syst. Sci. Discuss. 1–36. doi:10.5194/nhess-2016-75

Defant, A. 1940. Scylla e Cariddi e le correnti di marea nello Stretto di Messina. Geophisica Pura Applicata. 2:93.

Defant, A., Physical Oceanography, 2 volumes, Pergamon Press, New York (1961).

Del Ricco, R., 1982. Numerical model of the internal circulation of a strait under the influence of the tides, and its application to the Messina Strait, Nuovo Cimento,5C(1).

Di Sarra, A., Pace, A. Salusti, E., 1987. Long internal waves and columnar disturbances in the Strait of Messina, Journal of Geophysical Research. 92, 6495-6500.

Ford, R., Pain, C.C., Piggott, M.D., Goddard, A.J.H., de Oliveira, C.R.E., Umpleby, A.P., 2004a. A Nonhydrostatic Finite-Element Model for Three-Dimensional Stratified Oceanic Flows. Part II: Model Validation. Mon. Weather Rev. 132, 2832–2844. doi:10.1175/MWR2825.1

Ford, R., Pain, C.C., Piggott, M.D., Goddard, A.J.H., de Oliveira, C.R.E., Umpleby, A.P., 2004b. A Nonhydrostatic Finite-Element Model for Three-Dimensional Stratified Oceanic Flows. Part I: Model Formulation. Mon. Weather Rev. 132, 2816–2831. doi:10.1175/MWR2824.1

Friedrichs, C. T. and Aubrey, D. G. 1988. Non-linear Tidal Distortion in Shallow Well-mixed Estuaries: a Synthesis Estuarine, Coastal and Shelf Science. 27, 521-545

Hopkins, T.S., Salusti, E., Settimi, D., 1984. Tidal forcing of the water mass interface in the Strait of Messina. J. Geophys. Res. Ocean. 89, 2013–2024. doi:10.1029/JC089iC02p02013

Imasato, N., 1983. What is Tide-Induced Residual Current? J. Phys. Oceanogr. 13, 1307–1317. doi:10.1175/1520-0485(1983)013<1307:WITIRC>2.0.CO;2

Le Provost, C., G. Rougier and A. Poncet. 1981. NumericalModelling of the Harmonic Constituents of the Tides, with Application to the English Channel, Journal of Physical Oceanography, 11, pp.1123-1138.

Marshall, J., Adcroft, A., Hill, C., Perelman, L., Heisey, C., 1997. A finite-volume,incompressible Navier–Stokes model for, studies of the ocean on parallelcomputers. J. Geophys. Res. 102 (C3), 5753–5766.

Mosetti F. 1988. Some news on the currents in the Strait of Messina. Bollettino di Oceanologia, Teorica e Applicazioni; 6(3):119–76.

Pawlowicz, R., Beardsley, B., Lentz, S., 2002. Classical tidal harmonic analysis including error estimates in MATLAB using T_TIDE. Comput. Geosci. 28, 929–937. doi:10.1016/S0098-3004(02)00013-4

Piggott, M.D., Farrell, P.E., Wilson, C.R., Gorman, G.J., Pain, C.C., 2009. Anisotropic mesh adaptivity for multi-scale ocean modelling. Philos. Trans. R. Soc. London A Math. Phys. Eng. Sci. 367, 4591–4611.

Pope, S. B. 2000. Turbulent Flows. Cambridge University Press,. 80, 82, 84

Pugh, D.T. 1987. Tides, surges and mean sea-level: a handbook for engineers and scientists. Wiley, Chichester, 472pp.

Quattrocchi, A.; Gorman, J.G., Piggott M.D. and Cucco, A., 2016. M2, overtides and compound tides generation in the Strait of Messina: the response of a non-hydrostatic, finite-elemnt ocean model. In: Vila-Concejo, A.; Bruce, E.; Kennedy, D.M., and McCarroll, R.J. (eds.), Proceedings of the 14th International Coastal Symposium (Sydney, Australia). Journal of Coastal Research, Special Issue, No. 75, pp. XX-XX. Coconut Creek (Florida), ISSN 0749-0208.

Robinson IS. Tidally induced residual flows. In: Johns B, editor. Physical oceanography of coastal and shelf seas. Oceanographical Ser, vol. 35. Amsterdam: Elsevier; 1983. p. 321–56.

Sánchez-Garrido, J.C., Sannino, G., Liberti, L., García Lafuente, J., Pratt, L., 2011. Numerical modeling of three-dimensional stratified tidal flow over Camarinal Sill, Strait of Gibraltar. J. Geophys. Res. Ocean. 116.

Sannino, G., Carillo, A., Lombardi, E., Ciuffardi, T., 2013. Validazione del modello di circolazione Marina dello Stretto di Messina mediante dati acquisiti in situ.

Sannino, G., Carillo, A., Pisacane, G., Naranjo, C., 2015. On the relevance of tidal forcing in modelling the Mediterranean thermohaline circulation. Prog. Oceanogr. doi:10.1016/j.pocean.2015.03.002

Sapia A, Salusti E. Observation of nonlinear internal solitary wave trains at the northern and southern mouths of the Strait of Messina. Deep Sea Res 1987;34(7):1081–92.

Smagorinsky, J. 1963. General circulation experiments with the primitive equations. Monthly Weather Review. 91, 99–164.

Tee, K.T., 1977. Tide-Induced Residual Current—Verification of a Numerical Model. J. Phys. Oceanogr. 7, 396–402. doi:10.1175/1520-0485(1977)007<0396:TIRCOA>2.0.CO;2

Vercelli,F., Il regime delle correnti e delle maree nello stretto di Messina,Comm. Int. del Mediterraneo, Venice, Italy, 1925.

Xuan, J., Yang, Z., Huang, D., Wang, T., Zhou, F., 2015. Tidal residual current and its role in the mean flow on the Changjiang Bank. J. Mar. Syst. doi:10.1016/j.jmarsys.2015.04.005